A Variational Approach to the Evolution of Radial Basis Functions for Image Segmentation

Greg Slabaugh[1], Quynh Dinh[2], Gozde Unal[1]

[1]Intelligent Vision and Reasoning Department
Siemens Corporate Research
Princeton, NJ USA

{greg.slabaugh, gozde.unal}@siemens.com

[2]Computer Science Department
Stevens Institute of Technology
Hoboken, NJ USA

quynh@cs.stevens-tech.edu

Abstract

In this paper we derive differential equations for evolving radial basis functions (RBFs) to solve segmentation problems. The differential equations result from applying variational calculus to energy functionals designed for image segmentation. Our methodology supports evolution of all parameters of each RBF, including its position, weight, orientation, and anisotropy, if present. Our framework is general and can be applied to numerous RBF interpolants. The resulting approach retains some of the ideal features of implicit active contours, like topological adaptivity, while requiring low storage overhead due to the sparsity of our representation, which is an unstructured list of RBFs. We present the theory behind our technique and demonstrate its usefulness for image segmentation.

1. Introduction

Active contours have enjoyed copious success in computer vision since their introduction [7], and have since been the subject of intensive research activity. These methods have found application in numerous important problems such as image segmentation, 3D scene reconstruction, and object tracking. Part of their success is that they provide a structured approach (via energy minimization) to deform a contour or surface – a problem that comes up frequently in computer vision.

In the context of image segmentation, active contours deform based on various image-based and internal forces so that the contour's edges match object or region boundaries in the image, while maintaining smoothness. The smoothness, or regularization terms, provide robustness to noise while providing a measured approach to handling missing or low-confidence data. A typical application of an active contour will start with an initial contour, which is then itera-

tively deformed until it converges to a solution that balances the forces acting on the contour. Typically, these forces result from analytic expressions that are derived using variational calculus applied to an energy minimization problem; however, it is possible to define the forces directly without using an energy formulation.

In the active contour literature, earlier methods represented the contour using a topologically fixed parametric representation, such as a polyline, spline, etc., specified by a fixed number of control points. Such representations are simple and efficient to implement, however, they lack straightforward mechanisms for topological control. Often in segmentation problems, the topology of the problem is unknown a priori, and the contour must break apart or merge during evolution. While various authors have since presented methods that provide topological changes [8, 10, 5], the implementation is somewhat complicated and not natural to the parametric representation.

Recently there has been much interest in implicit active contours, or level set methods, which represent the surface as a level set of a higher dimensional embedding function [1, 2, 14, 16]. The primary advantage of this representation is that topological changes occur naturally in this framework; by manipulating the embedding function, the level set that represents the contour can innately split or merge without requiring any specialized implementation to handle topological changes. However, the embedding function must be updated on a dense set of points, requiring significant storage, even when using efficient narrowband techniques [9].

Even more recently, there has been much interest in combining some of the advantages of explicit and implicit active contours through the use of radial basis functions (RBFs) [11, 12] (these papers are the source of inspiration for this work) or unstructured point clouds [6]. These methods define a set of points (or RBFs), from which the

embedding function can be computed. These approaches then, provide a methodology to move the points (and correspondingly, update the embedding function) to deform the active contour to solve the segmentation problem. Such approaches have been demonstrated to provide the topological flexibility of level set methods with the low storage requirements of parametric representations, and offer much flexibility in terms of RBF placement and interaction.

This paper is related to such work; however, there are notable differences. These previous methods start with the force definition rather than deriving the forces through an energy formulation. We present this derivation, which provides a stronger theoretical framework for the technique. In addition, from this derivation we observe how it is possible to evolve *all* attributes of each RBF, whereas previous work only evolved the RBF positions. For example, in the case of an anisotropic Gaussian RBF interpolant, we show how to evolve the position, weight, orientation, and standard deviations of each RBF, resulting in a set of coupled differential equations that drive the active contour. In addition, we derive equations for region-based segmentation problems in addition to the edge-based segmentation problems addressed previously. Our methodology is general, allowing other RBF interpolants and curve evolutions to be utilized in our framework.

The rest of this paper is organized as follows. In Section 2 we present the mathematical details of our framework, deriving the RBF update equations from an energy functional. Next, in Section 3 we complete the derivation by considering anisotropic radial basis functions. Then, in Section 4 we provide some implementation details, including how we add and merge RBFs during evolution. In Section 5 we show some initial results that demonstrate the usefulness of our method, and offer some concluding remarks in Section 6.

2. Variational RBF Evolution

In this section we derive our RBF evolution equations, resulting in a set of coupled differential equations that drive the evolution. We begin by considering region-based image segmentation.

2.1. Region-based image segmentation

In region-based segmentation methods, the evolution of the active contour is based on the attributes of entire regions in the image. These attributes can include intensity, color, texture, probabilities, etc., but in this paper we focus on intensity. These methods model the image as being composed of distinct regions, each with its own statistics, which are used to deform the active contour towards the region boundaries. This is notably different than boundary-based segmentation methods, where the evolution depends on lo-

cal image gradients. In this sense, region-based segmentation methods are more global and more robust to noise than edge-based methods.

Perhaps the most well-known region-based model is the Mumford-Shah functional [13], which models the image regions as piece-wise smooth functions. For example, in the case of two regions R inside the contour C and the region R^C outside the contour,

$$
E(f, C) = \int_R (I(\mathbf{x}) - f_R(\mathbf{x}))^2 d\mathbf{x} \tag{1}
$$
$$
+ \int_{R^C} (I(\mathbf{x}) - f_{R^C}(\mathbf{x}))^2 d\mathbf{x} + \int_{\Omega \setminus C} |\nabla f|^2 d\mathbf{x} + \gamma \int_C ds,
$$

where $E(f, C)$ is the energy of the contour, $I(\mathbf{x})$ is the image intensity at pixel $\mathbf{x}$, and f is a piecewise smooth function, consisting of regions $f_R(\mathbf{x})$ inside C and $f_{R^C}(\mathbf{x})$ outside C, and the last term is a regularization term weighted by a constant γ. While there are good active contour methods to solve the Mumford-Shah functional [17], the piecewise constant model of Chan-Vese [2] is a powerful approximation that replaces the piecewise smooth function f with piecewise constant functions in each region. This simplified form can be expressed as

$$
E(C) = \int_R (I(\mathbf{x}) - \mu_{in})^2 d\mathbf{x} + \int_{R^C} (I(\mathbf{x}) - \mu_{out})^2 d\mathbf{x} + \gamma \int_C ds, \tag{2}
$$

where μ_{in} is the average intensity inside the C and μ_{out} is the average intensity outside C. Many other variations of the Chan-Vese functional exist, for example, using various statistics other than or in addition to the mean.

In both the level set formulation and ours based on RBFs, the contour $C \in \Omega$ is represented by the zero level set of a Lipschitz function $\phi : \Omega \to \Re$, such that

$$
\begin{aligned}
C &= \{\mathbf{x} \in \Omega : \phi(\mathbf{x}) = 0\}, \\
R &= \{\mathbf{x} \in \Omega : \phi(\mathbf{x}) < 0\}, \\
R^C &= \{\mathbf{x} \in \Omega : \phi(\mathbf{x}) > 0\}
\end{aligned}
$$

Now in our case, we model the embedding function $\phi(\mathbf{x})$ using N radial basis functions $\psi(\mathbf{x}, g_{i1} \cdots g_{iM})$ [18] as

$$
\phi(\mathbf{x}) = P(\mathbf{x}) + \sum_{i=1}^{N} w_i \psi_i(\mathbf{x}, g_{i1} \cdots g_{iM}), \tag{3}
$$

where $\psi_i(\mathbf{x}, g_{i1} \cdots g_{iM})$ is the ith RBF parameterized by M variables $g_{i1} \cdots g_{iM}$, w_i is the weight on the ith RBF, and $P(\mathbf{x})$ is a polynomial term that spans the null space of the basis function.

Using the Heaviside function,

$$
H(z) = \begin{cases} 1, & z \geq 0 \\ 0, & \text{otherwise} \end{cases} \tag{4}
$$

and the Dirac delta function $\delta(z) = \frac{d}{dz}H(z)$, the energy of Equation 2 can be reexpressed as

$$E(\phi(\mathbf{w}, \mathbf{g})) = \int_\Omega (I(\mathbf{x}) - \mu_{in})^2 H(\phi(\mathbf{x}))d\mathbf{x} \qquad (5)$$
$$+ \int_\Omega (I(\mathbf{x}) - \mu_{out})^2 (1 - H(\phi(\mathbf{x})))d\mathbf{x} + \gamma \int_\Omega \delta(\phi(\mathbf{x}))|\nabla\phi(\mathbf{x})|d\mathbf{x},$$

where $\mathbf{w} = [w_1 \ldots w_N]^T$, and $\mathbf{g} = [g_{ij}]$, where $i = 1 \cdots N, j = 1 \cdots M$.

Under this formulation of the problem, we would like to derive the variation of the energy with respect to the RBF parameter g_{ij}, as well as the RBF weight, w_i. Using the chain rule, we derive

$$\frac{\partial E}{\partial g_{ij}} = \int_\Omega (I(\mathbf{x}) - \mu_{in})^2 \delta(\phi(\mathbf{x})) \frac{\partial\phi}{\partial g_{ij}} d\mathbf{x}$$
$$- \int_\Omega (I(\mathbf{x}) - \mu_{out})^2 \delta(\phi(\mathbf{x})) \frac{\partial\phi}{\partial g_{ij}} d\mathbf{x}$$
$$+ \gamma \int_\Omega \mathrm{div}\left(\frac{\nabla\phi}{|\nabla\phi|}\right) \delta(\phi(\mathbf{x})) \frac{\partial\phi}{\partial g_{ij}} d\mathbf{x}, \quad (6)$$

which simplifies to the contour integral,

$$\frac{\partial g_{ij}}{\partial t} = \frac{\partial E}{\partial g_{ij}} = \int_C \left[(I(\mathbf{x}) - \mu_{in})^2 - (I(\mathbf{x}) - \mu_{out})^2\right.$$
$$\left. + \gamma\mathrm{div}\left(\frac{\nabla\phi}{|\nabla\phi|}\right)\right] \frac{\partial\phi}{\partial g_{ij}} dC, \qquad (7)$$

and similarly,

$$\frac{\partial w_i}{\partial t} = \frac{\partial E}{\partial w_i} = \int_C \left[(I(\mathbf{x}) - \mu_{in})^2 - (I(\mathbf{x}) - \mu_{out})^2\right.$$
$$\left. + \gamma\mathrm{div}\left(\frac{\nabla\phi}{|\nabla\phi|}\right)\right] \frac{\partial\phi}{\partial w_i} dC. \qquad (8)$$

We note that these expressions take the form $\int_C \frac{\partial E}{\partial\phi}\frac{\partial\phi}{\partial p}dC$, where p is g_{ij} or w_i. This form results from the functional composition that resulted in application of the chain rule. Conceptually, these equations state that to determine the update of a parameter of an RBF, we must traverse the contour C, accumulating gradients at each point. That is, each point on the zero level set contributes to the update of the RBF parameters, which is intuitive, given that in general, the RBF influences every point on the zero level set. Unlike standard level set update equations, the integral in Equations 7 and 8 combines measurements from all points along the contour [15], providing increased robustness to noise. We note that our formulation of the problem is notably different than [11], where the RBFs are fixed to the zero level set and the evolution of an RBF does not consider the influence of the RBF on all other points on the zero level set. Likewise, this approach differs from [12] as it is based solely on gradient descent and does not require

solving linear systems of equations for the RBF locations. Unlike [11, 12, 6], our method provides a generalized simple way to update *all* parameters of the basis function, including the weights, position, orientation, anisotropy, etc. This of course depends on the functional form of ϕ, for which we consider for various basis functions in Section 3. We note that each iteration of all RBFs is order $O(LMN)$, where L is the number of pixels on the zero level set, and M and N are given above.

2.2. Boundary-based image segmentation

From the previous section, we observed that the energy minimization resulted in the form $\int_C \frac{\partial E}{\partial\phi}\frac{\partial\phi}{\partial p}dC$. In general, one can utilize this relationship to transform any level set flow or curve evolution into an RBF evolution in our framework. For boundary-based image segmentation, we deduce a similar expression for the geodesic flow [1],

$$\frac{\partial g_{ij}}{\partial t} = \frac{\partial E}{\partial g_{ij}} = \int_C [F\kappa|\nabla\phi| - \nabla F \cdot \nabla\phi] \frac{\partial\phi}{\partial g_{ij}} dC$$
$$\frac{\partial w_i}{\partial t} = \frac{\partial E}{\partial w_i} = \int_C [F\kappa|\nabla\phi| - \nabla F \cdot \nabla\phi] \frac{\partial\phi}{\partial w_i} dC,$$

where $F(I(\mathbf{x}))$ is a function of an edge detector response, such as $F = \frac{1}{1+|\nabla I|^2}$ and κ is the curvature of the active contour at point $\mathbf{x}$. We note often with boundary-based segmentations, it is helpful to run a GVF diffusion [20] on the vector field ∇F before evolving the active contour.

3. Radial Basis Functions

In the previous section, we derived the basic equations for evolution of radial basis functions to achieve either a region-based or boundary-based image segmentation. However, the complete derivation depends on the RBFs chosen and their derivatives. In this section, we consider the use of anisotropic Gaussian RBFs. We note however, that our framework is quite general, and that any RBF with an analytic derivative can be used. We choose to work with anisotropic basis functions for two reasons: first, they can better approximate sharp corners [4], and second, they are a more general form of the isotropic basis function. Also note that in the presentation below we consider 2D RBFs, however, the method straightforwardly generalizes to 3D.

3.1. Anisotropic Gaussian RBFs

The equation for a 2D anisotropic Gaussian centered at point (c_x, c_y), standard deviation σ_x, σ_y, and orientation angle θ has the functional form

$$\psi(x, y) = \frac{1}{2\pi\sigma_x\sigma_y} \exp\left[\frac{-1}{2\sigma_x^2\sigma_y^2}\left(a_1(x - c_x)^2\right.\right.$$
$$\left.\left. -2a_2(x - c_x)(y - c_y) + a_3(y - c_y)^2\right)\right],$$

where

$$a_1 = \sigma_x^2 \cos^2\theta + \sigma_y^2 \sin^2\theta \tag{9}$$

$$a_2 = (\sigma_y^2 - \sigma_x^2)\cos\theta\sin\theta \tag{10}$$

$$a_3 = \sigma_x^2 \sin^2\theta + \sigma_y^2 \cos^2\theta \tag{11}$$

This RBF is described by the $M = 5$ five parameters, $g_j = [c_x, c_y, \sigma_x, \sigma_y, \theta]^T$. To implement our RBF flows, we must take the derivative of the RBF with respect to these parameters. Doing so yields the equations,

$$\frac{\partial\psi}{\partial c_x} = \psi \cdot \left(\frac{a_1 X - a_2 Y}{\sigma_x^2 \sigma_y^2}\right) \tag{12}$$

$$\frac{\partial\psi}{\partial c_y} = \psi \cdot \left(\frac{-a_2 X + a_3 Y}{\sigma_x^2 \sigma_y^2}\right) \tag{13}$$

$$\frac{\partial\psi}{\partial\theta} = \psi \cdot \left(-\frac{X^2 \frac{\partial a_1}{\partial\theta} - 2XY\frac{\partial a_2}{\partial\theta} + Y^2 \frac{\partial a_3}{\partial\theta}}{2\sigma_x^2 \sigma_y^2}\right) \tag{14}$$

$$\frac{\partial\psi}{\partial\sigma_x} = -\frac{\psi}{\sigma_x} + \psi \cdot \left[\frac{a_1 X^2 - 2a_2 XY + a_3 Y^2}{\sigma_x^3 \sigma_y^2}\right.$$
$$\left. -\frac{1}{2\sigma_x^2 \sigma_y^2}\left(X^2\frac{\partial a_1}{\partial\sigma_x} - 2XY\frac{\partial a_2}{\partial\sigma_x} + Y^2\frac{\partial a_3}{\partial\sigma_x}\right)\right] \tag{15}$$

$$\frac{\partial\psi}{\partial\sigma_y} = -\frac{\psi}{\sigma_y} + \psi \cdot \left[\frac{a_1 X^2 - 2a_2 XY + a_3 Y^2}{\sigma_x^2 \sigma_y^3}\right.$$
$$\left. -\frac{1}{2\sigma_x^2 \sigma_y^2}\left(X^2\frac{\partial a_1}{\partial\sigma_y} - 2XY\frac{\partial a_2}{\partial\sigma_y} + Y^2\frac{\partial a_3}{\partial\sigma_y}\right)\right], \tag{16}$$

where

$$X = (x - c_x) \tag{17}$$

$$Y = (x - c_y) \tag{18}$$

$$\frac{\partial a_1}{\partial\theta} = -2(\sigma_x^2 - \sigma_y^2)\cos\theta\sin\theta \tag{19}$$

$$\frac{\partial a_2}{\partial\theta} = -(\sigma_x^2 - \sigma_y^2)(\cos^2\theta - \sin^2\theta) \tag{20}$$

$$\frac{\partial a_3}{\partial\theta} = 2(\sigma_x^2 - \sigma_y^2)\cos\theta\sin\theta \tag{21}$$

$$\frac{\partial a_1}{\partial\sigma_x} = 2\sigma_x \cos^2\theta \tag{22}$$

$$\frac{\partial a_2}{\partial\sigma_x} = -2\sigma_x \cos\theta\sin\theta \tag{23}$$

$$\frac{\partial a_3}{\partial\sigma_x} = 2\sigma_x \sin^2\theta \tag{24}$$

$$\frac{\partial a_1}{\partial\sigma_y} = 2\sigma_y \sin^2\theta \tag{25}$$

$$\frac{\partial a_2}{\partial\sigma_y} = 2\sigma_y \cos\theta\sin\theta \tag{26}$$

$$\frac{\partial a_3}{\partial\sigma_y} = 2\sigma_y \cos^2\theta \tag{27}$$

$$\tag{28}$$

Putting it all together gives the following set of coupled ordinary differential equations (ODEs) that drive the ith RBF:

$$\frac{dc_{ix}}{dt} = \int_C D w_i \psi_i \cdot \left(\frac{a_{i1} X_i - a_{i2} Y_i}{\sigma_{ix}^2 \sigma_{iy}^2}\right) dC \tag{29}$$

$$\frac{dc_{iy}}{dt} = \int_C D w_i \psi_i \cdot \left(\frac{-a_{i2} X_i + a_{i3} Y_i}{\sigma_{ix}^2 \sigma_{iy}^2}\right) dC \tag{30}$$

$$\frac{dw_i}{dt} = \int_C D\psi_i dC \tag{31}$$

$$\frac{d\theta_i}{dt} = \int_C D w_i \cdot$$
$$\psi_i \cdot \left(-\frac{X_i^2 \frac{\partial a_{i1}}{\partial\theta_i} - 2X_i Y_i \frac{\partial a_{i2}}{\partial\theta_i} + Y_i^2 \frac{\partial a_{i3}}{\partial\theta_i}}{2\sigma_{ix}^2 \sigma_{iy}^2}\right) dC \tag{32}$$

$$\frac{d\sigma_{ix}}{dt} = \int_C D w_i \cdot$$
$$\left\{-\frac{\psi_i}{\sigma_{ix}} + \psi_i \cdot \left[\frac{a_{i1} X_i - 2a_{i2} X_i Y_i + a_{i3} Y_i^2}{\sigma_{ix}^3 \sigma_{iy}^2}\right.\right.$$
$$\left.\left. -\frac{1}{2\sigma_{ix}^2 \sigma_{iy}^2}\left(X_i^2\frac{\partial a_{i1}}{\partial\sigma_{ix}} - 2X_i Y_i\frac{\partial a_{i2}}{\partial\sigma_{ix}} + Y_i^2\frac{\partial a_{i3}}{\partial\sigma_{ix}}\right)\right]\right\} dC \tag{33}$$

$$\frac{d\sigma_{iy}}{dt} = \int_C D w_i \cdot$$
$$\left\{-\frac{\psi_i}{\sigma_{iy}} + \psi_i \cdot \left[\frac{a_{i1} X_i^2 - 2a_{i2} X_i Y_i + a_{i3} Y_i^2}{\sigma_{ix}^2 \sigma_{iy}^3}\right.\right.$$
$$\left.\left. -\frac{1}{2\sigma_{ix}^2 \sigma_{iy}^2}\left(X_i^2\frac{\partial a_{i1}}{\partial\sigma_{iy}} - 2X_i Y_i\frac{\partial a_{i2}}{\partial\sigma_{iy}} + Y_i^2\frac{\partial a_{i3}}{\partial\sigma_{iy}}\right)\right]\right\} dC \tag{34}$$

where

$$X_i = (x - c_{ix}) \tag{35}$$

$$Y_i = (y - c_{iy}) \tag{36}$$

and for region-based segmentation,

$$D = \left[(I(\mathbf{x}) - \mu_{in})^2 - (I(\mathbf{x}) - \mu_{out})^2 + \gamma\text{div}\left(\frac{\nabla\phi}{|\nabla\phi|}\right)\right] \tag{37}$$

while for boundary-based segmentation,

$$D = [F\kappa|\nabla\phi| - \nabla F \cdot \nabla\phi] \tag{38}$$

While these systems of equations may look complex, they contain many repeated terms and are easily implemented on a computer.

A simple example demonstrating RBF evolutions using these ODEs is provided for a synthetic image in Figure 1. In this example, a white square, containing sharp corners, is to be segmented from the black background. In (a) of the
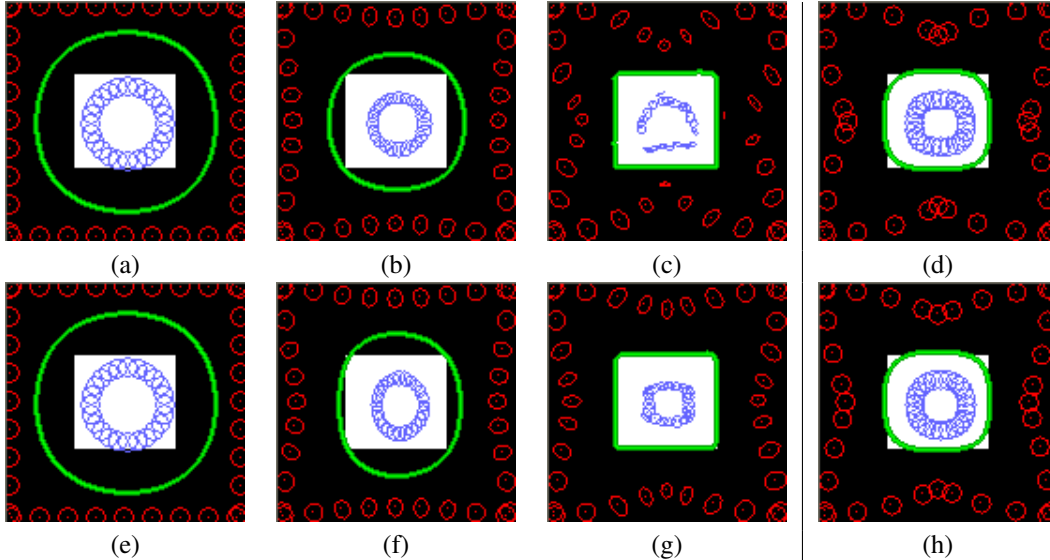
Figure 1. RBF evolution for segmentation of a white square on a black background. Top row: Chan-Vese region-based flow. Bottom row: geodesic boundary-based flow. The evolution is shown starting at initialization ((a) and (e)), at an intermediate stage ((b) and (f)), and at convergence ((c) and (g)) for the evolution of all RBF parameters, including anisotropy. For comparison, in (d) and (h) we show the isotropic RBF evolution result of evolving just the weights and RBF centers. The isotropic RBFs are unable to capture the sharp corners of the object.

figure, we show the initialization, which consists of a contour, shown in green, which is the zero level set of the implicit function $\phi(x, y)$. The implicit function is represented as a summation of RBFs. Negative weighted RBFs are rendered in blue, while positive weighted RBFs are rendered in red. The ellipse around each RBF is a visualization of the anisotropy. Initially, the RBFs are all isotropic and are rendered as circles. In (b), we show the result at an intermediate stage of the segmentation after 10 iterations of the ODEs and in (c), we show the final result after convergence after 25 iterations. Note the RBFs changed their positions, weights, and anisotropy to produce the result in (c), which provides an excellent segmentation of the data. For comparison, in (d) we show the evolution of just the RBF weights and center positions. In this case, the isotropic RBFs are unable to capture the sharp corners of the object. The bottom row of the figure reruns this experiment using the geodesic boundary based flow, which provides similar results.

3.2. Other Basis Functions

We note any RBF interpolant that has an analytic derivative can be used in our framework, including multi-order [3] and Wendland's [19] RBFs. Experimentally, we have observed best results using RBFs that decay from their center location. However, due to page constraints we do not present derivations or results for these other RBFs.

4. Implementation

In this section, we provide some implementation details regarding our RBF evolution approach to image segmentation.

4.1. Overall approach

Our approach requires an initialization, which consists of a set of RBFs that define an initial contour for segmentation. The positions of these RBFs can be placed manually by the user, or automatically by placing positive-weighted RBFs on the image border or in a large ring around the image center, and negative-weighted RBFs in the center of the image, resulting in an initial contour on the image. The initialization is flexible, as the initial contour can be inside, outside, or both inside and outside the object being segmented, as we will show in the examples of Section 5. Given this initial contour, we then evolve the RBFs using Equations 29 to 34. These ODEs update the RBF parameters, and consequently update the curve as well to solve the segmentation problem. One can check for convergence of the ODEs by monitoring the energy of E.

4.2. Merging and adding RBFs

We additionally include a mechanism to merge or add RBFs, which we execute periodically during the RBF evolution. In the case of a merge, let the ith RBF be parameterized by $[c_{ix}, c_{iy}, \sigma_{ix}, \sigma_{iy}, \theta_i]$ and weight w_i, and
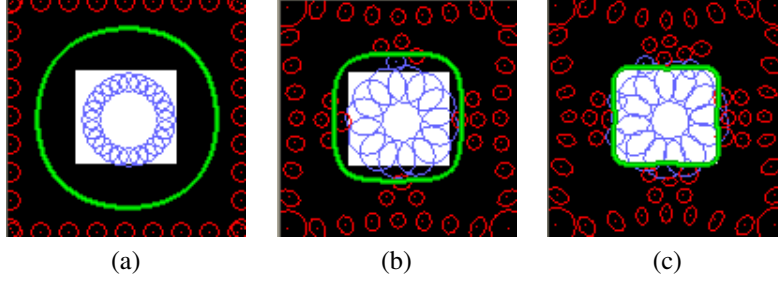
(a)　　　　　　　　(b)　　　　　　　　(c)

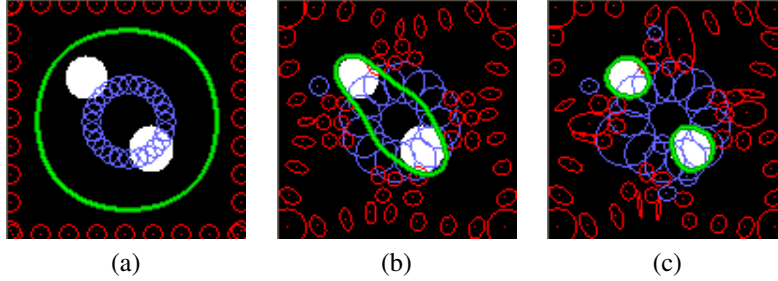Figure 2. Adding and removing RBFs.

(a)　　　　　　　　(b)　　　　　　　　(c)

Figure 3. An example demonstrating a topological change of the contour.

the jth RBF by $[c_{jx}, c_{jy}, \sigma_{jx}, \sigma_{jy}, \theta_j]$ and weight w_j, $i \neq j$. If the distance between two RBFs, $d_{ij} = \sqrt{(c_{ix} - c_{jx})^2 + (c_{iy} - c_{jy})^2}$ becomes less than a threshold T_M (typically 7 pixels in our experiments), then the RBFs are combined by deleting them and replacing them with a new RBF, $[\frac{1}{2}(c_{ix} + c_{jx}), \frac{1}{2}(c_{iy} + c_{jy}), \sigma_{ix} + \sigma_{jx}, \sigma_{iy} + \sigma_{jy}, \theta_i + \theta_j]$ and weight $w_i + w_j$. This new RBF is a sum of the two RBFs being merged and centered halfway between.

We add RBFs at locations where the gradient of the implicit function is high. However, we do not want to add an RBF too close to an already existing RBF. To satisfy these constraints, we form a function $A(x, y) = \frac{\nabla \phi(x,y)}{\max(\nabla \phi(x,y))} \cdot S(x, y)$, where $\frac{\nabla \phi(x,y)}{\max(\nabla \phi(x,y))}$ is the normalized gradient of the implicit function and $S(x, y)$ is a splat buffer formed as

$$ S(x, y) = \prod_i \left(1 - e^{-[(c_{ix} - x)^2 + (c_{iy} - y)^2]/(2\sigma^2)} \right) \quad (39) $$

where σ is a standard deviation of a 2D Gaussian function (set to 15 for our experiments). The splat buffer is close to one where there are no RBFs, and decreases to zero near RBF centers. Therefore, the function $A(x, y)$ is large where there are no RBFs and the gradient of the implicit function is high. We scan $A(x, y)$, and add an RBF at the position (x, y) where $A(x, y)$ has a value above a threshold, T_A (typically 0.65 in our experiments). This gives us a new RBF that is not too close to an existing RBF, yet is located at a point of high gradient in the implicit function. The threshold T_A prevents us from adding too many constraints where they are not really needed. The weight of this newly added

isotropic RBF is initially zero; subsequent iterations of the ODEs will update its weight and anisotropy.

An example showing the adding and merging of RBFs is provided in Figure 2. Here, the method automatically places the RBFs where they will help the most in modeling the curve geometry, and ODEs update the RBFs to solve the segmentation problem. Using these mechanisms, topological changes of the contour also come naturally in our framework. An example of this is provided in Figure 3.

5. Results

In this section we present some results demonstrating the effectiveness of our proposed method in segmentation of various images.

In Figure 4, we repeat the experiment of Figure 2, this time on a very noisy image corrupted by Gaussian white noise. Here the image was formed by setting the background pixels to 0, the foreground pixels to 200, and adding in Gaussian white noise of unit standard deviation, where the noise was then multiplied by 200. The resulting image was clipped to [0, 255], and has a very noisy appearance. The evolution of our anisotropic RBFs are shown from the initialization (a), at an intermediate stage (b), and upon convergence (c). The region-based active contour does an excellent job of segmenting the object despite the low signal to noise ratio. In each of these examples, we set $\gamma = 0$ as the basis functions themselves are already quite smooth.

In Figure 5, we apply our RBF segmentation method to an ultrasound fetal image. The brighter structure is part of
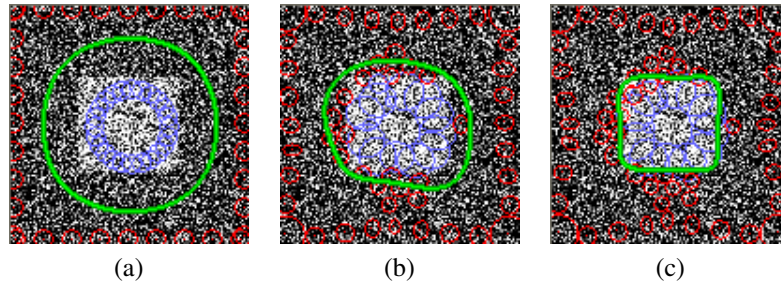
Figure 4. Segmentation of a noisy image. In (a) through (c), we show the evolution of anisotropic RBFs at different time steps until convergence (c). Despite the noise, the RBF active contour is able to adequately segment the image.

the fetal anatomy. From the initialization shown in (a) of the figure, we evolve our active contour for 10 iterations (b), 20 iterations (c), and show the result upon convergence (25 iterations), shown in (d). The segmentation successfully delineates the anatomic fetal structure.

Figure 6 demonstrates our method with numerous images. Starting with the upper left part of the figure, we show the segmentation of a CT image, where we would like to segment the bone in the center of the image. Placing some negative weighted constraints inside the bone, and positive constraints outside, we get an initial contour shown in (a). Using our method, we evolve the RBFs until convergence, producing the result shown in (b). In (c) we perform a similar experiment using a T1-weighted MR image of a lymph node, which appears as a darkish object in the center of the image. The converged result is shown in (d), which provides an excellent segmentation of this object.

In (e) and (f) we present an example of a photographic image taken of a highway. Starting with an initial contour as depicted in (e), we evolve the RBFs until convergence, producing the result in (f). The segmentation is successful as it depicts the two cars; however, the result is not perfect as the Chan-Vese model we employ assumes that the image has a bimodal histogram with piece-wise constant regions, which is not the case for this image. A different image model, such as one based on non-parametric density estimation, would likely produce better results for this image. Any such curve evolution can be incorporated into our framework; however, this is left for future work. Also note that this example also demonstrates a topological split of the contour, which is needed to model the two separate objects. Finally, in (g) and (h) we show an example segmentation of a blood vessel from an angiography image. Starting with a small contour in the center, the contour grows outward along the vessel boundaries, providing an excellent segmentation result.

6. Conclusion

In this paper we presented a variational framework for evolving radial basis functions for active contour image segmentation. From an energy formulation, we derived differ-

ential equations for updating the RBF constraints so that they deform an active contour to achieve the segmentation. From our derivation, we presented a simple way to evolve *all* of the parameters associated with the RBF, including the constraint centers, weights and anisotropy. The RBFs are not constrained to the contour location and only require minimal storage for evolution. We demonstrated the method's effectiveness by segmenting several images.

For future work we are interested in implementing the method in 3D and comparing results obtained with different radial basis functions as well as different functionals for image segmentation. Furthermore, we believe the theory underlying this paper will be useful in other applications, such as filtering, tracking, and registration; we plan on investigating these topics in the future.

References

[1] V. Casselles, R. Kimmel, and G. Saprio. Geodesic Active Contours. *The Intl. Journal of Computer Vision*, 22(1):61–79, 1997.

[2] T. Chan and L. Vese. Active Contours Without Edges. *IEEE Trans. on Image Processing*, 10(2):266–277, 2001.

[3] F. Chen and D. Suter. Multiple Order Laplacian Splines - Including Splines with Tension. Technical report, Monash University, Department of Electrical and Computer Systems Engineering, 1996.

[4] H. Q. Dinh, G. Turk, and G. Slabaugh. Reconstructing Surfaces Using Anisotropic Basis Functions. In *International Conference on Computer Vision (ICCV)*, pages 606–613, 2001.

[5] Y. Duan, L. Yang, H. Qin, and D. Samaras. Shape Reconstruction from 3D and 2D Data Using PDE-Based Deformable Surfaces. In *ECCV*, volume III, pages 238–251, 2004.

[6] H. Ho, Y. Chen, H. Liu, and P. Shi. Level Set Active Contours on Unstructured Point Clouds. In *CVPR*, pages 690–697, 2005.

[7] M. Kass, A. Witkin, and D. Terzopoulos. Snakes: Active Contour Models. *Intl. Journal of Computer Vision*, 1(4):321–331, 1987.
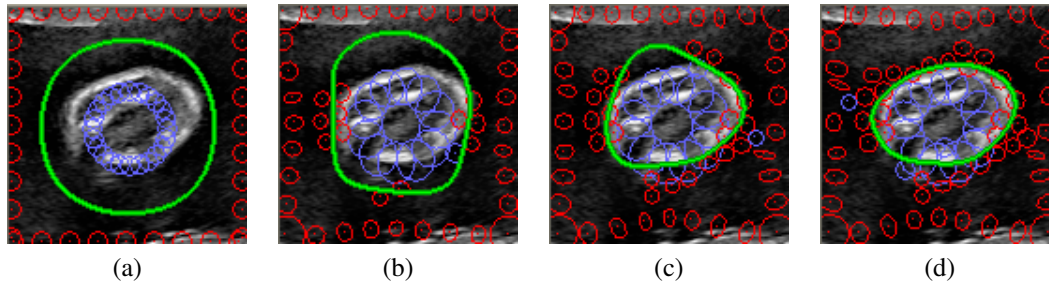
(a)   (b)   (c)   (d)

Figure 5. Segmentation of an ultrasound image. In (a) through (d), we show the evolution of anisotropic RBFs at different time steps until convergence (d).

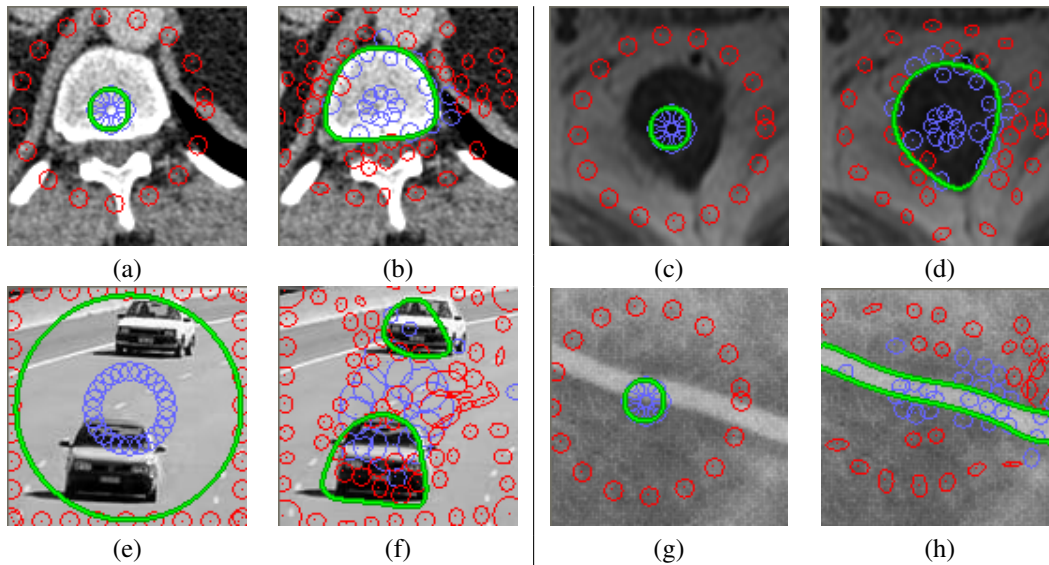(a)   (b)   (c)   (d)

(e)   (f)   (g)   (h)

Figure 6. More examples. For each example, we show the initialization and the converged result. In (a) and (b): a CT bone image, (c) and (d): an MR lymph node image, (e) and (f): a photographic image of a highway, (g) and (h): an x-ray angiography image.

[8] J. Lachaud and J.Montanvert. Deformable Meshes with Automated Topology Changes for Coarse-To-Fine 3D Surface Extraction. *Medical Image Analysis*, 3(2):187–207, 1999.

[9] R. Malladi, J. Sethian, and B. Vemuri. Shape Modeling With Front Propagation: A Level Set Approach. *IEEE Trans. on Patt. Anal. and Machine Intelligence*, 17(2):158–175, 1995.

[10] T. McInerney and D. Terzopoulos. Topology Adaptive Deformable Surfaces for Medical Image Volume Segmentation. *IEEE Trans. on Medical Imaging*, 18(10):840–850, 1999.

[11] B. Morse, W. Liu, T. Yoo, and K. Subramanian. Active Contours Using a Constraint-Based Implicit Representation. In *CVPR*, pages 285–292, 2005.

[12] M. Mullan, R. Whitaker, and J. Hart. Procedural Level Sets. In *NSF/DARPA CARGO Meeting*, 2004.

[13] D. Mumford and J. Shah. Optimal Approximation by Piecewise Smooth Functions and Associated Variational Problems. *Commun. Pure Appl. Math*, 42:577–685, 1989.

[14] S. Osher and J. A. Sethian. Fronts Propagating with Curvature-Dependent Speed: Algorithms Based on Hamilton–Jacobi Formulations. *Journal of Computational Physics*, 79:12–49, 1988.

[15] M. Rochery, I. Jermyn, and J. Zerubia. Higher Order Active Contours. *International Journal of Computer Vision*, 69(1):27–42, 2006.

[16] J. A. Sethian. *Level Set Methods and Fast Marching Methods Evolving Interfaces in Computational Geometry, Fluid Mechanics, Computer Vision, and Materials Science*. Cambridge University Press, 1999.

[17] A. Tsai, A. Yezzi, and A. Willsky. Curve Evolution Implementation of the MumfordShah Functional for Image Segmentation, Denoising, Interpolation, and Magnification. *IEEE Trans. Image Process.*, 10(8):1169–1186, 2001.

[18] G. Turk and J. O'Brien. Shape Transformation using Variational Implicit Surfaces. In *SIGGRAPH 99 Proceedings*, pages 335–342, 1999.

[19] H. Wendland. *Scattered Data Approximation*. Cambridge Monographs on Applied and Computational Mathematics, 2005.

[20] C. Xu and J. L. Prince. Snakes, shapes, and gradient vector flow. *IEEE Trans. Image Process.*, 7(3):359–369, 1998.